# Development of an *in vitro* senescent hepatic cell model for metabolic studies in aging

Authors/Affiliations

Brijesh Kumar Singh[1*], Madhulika Tripathi[1], Reddima Sandireddy[1], Keziah Tikno[1], Jin Zhou[1] and Paul Michael Yen[1,2]

[1]Cardiovascular and Metabolic Disorders Program, Duke-NUS Medical School, Singapore 169857

[2]Duke University School of Medicine, Durham, NC 27710, USA

Contact

Cardiovascular and Metabolic Disorders Program, Duke-NUS Medical School, Singapore 169857. Email: singhbrijeshk@duke-nus.edu.sg, Telephone: +65-6516 7666.

Abstract

Although in vitro senescence models have been developed using primary fibroblasts, they may not be applicable for the study of metabolically active organs such as the liver. We thus developed an *in vitro* protocol to induce senescence in AML12 nontransformed hepatocyte cell lines derived from mice transgenic for transforming growth factor alpha. Sequential oxidative stress with hydrogen peroxide induced premature senescence in these cells as they exhibited molecular and metabolic signatures, had increased SA-βGal and γH2A.X staining, and elevated senescence and pro-inflammatory gene expression that resembled the livers from aged mice. Metabolic phenotyping showed fuel switching towards more glycolysis, mitochondrial glutamine oxidation, and impaired energy production that also was similar to the livers from aged mice. Additionally, Senescence Activated Secretory Proteins (SASPs) sensitized normal AML12 cells to palmitate-induced toxicity, a known pathological effect of hepatic aging. In summary, we have generated an *in vitro* senescent AML12 cell model that not only show the molecular hallmarks of aging, but also recapitulates the aberrant metabolic phenotype found in aged liver. As such, they represent a novel and useful model to study nutritional, pharmacological, or genetic factors on hepatic metabolism during aging.

Keywords

Aging, Liver, Senescence, Metabolism, AML12 cells

## INTRODUCTION

Aging is a major risk factor for many chronic diseases. In the liver, aging increases the susceptibility towards acute liver injury and hepatic fibrotic response [1-3]. Moreover, aging has been positively associated with increased risk and poor prognosis of various liver diseases including non-alcoholic fatty liver disease (NAFLD), alcoholic liver disease, hepatitis C, and negatively associated with hepatic regenerative capacity [3, 4]. Thus, the study of aging and chronic hepatic diseases has been hampered by the long period of time necessary to conduct human and animal studies, and the limited relevance of non-mammalian models to human diseases. While there are *in vitro* aging models that employ fibroblasts, there currently is an urgent need for *in vitro* models to study aging in the liver.

Cellular senescence in the main feature manifested in tissues of the aging organism [1, 5-8]. It is characterized by permanent cell cycle arrest, resistance to apoptosis, and a senescence-associated secretory phenotype [5]. Under pathological stress conditions, excessive accumulation of senescence cells in affected tissues adversely affects the tissue's regenerative ability and creates a pro-inflammatory environment that can resemble various age-related disorders such as Alzheimer's disease, cancer, arthritis, cataracts, osteoporosis, atherosclerosis, hypertension, cardiovascular disease, Type 2 diabetes, and chronic liver disorders [3, 5, 7, 9-12]. Targeting senescent cells has the potential to delay age-associated disorders and/or reverse pathological metabolic phenotypes [3, 13-16]. Recent studies in the liver show that inducing hepatocyte senescence promotes fat accumulation and hepatic steatosis *in vitro* and *in vivo* [17]. Likewise, targeting senescent hepatocytes and adipocytes reduce overall hepatic steatosis and improve

obesity-induced metabolic dysfunction [14, 17]. These findings suggest that senescence plays an important role in the development of chronic hepatic diseases and their metabolic abnormalities. The development of *in vitro* models of hepatic cell senescence would enable more detailed and mechanistic analysis of the molecular, cellular signalling, and metabolic changes that occur in senescence and how drugs and environmental factors may affect it.

Previous senescence cell models have used primary fibroblast or hepatic cancer cells subjected to oxidative stress [18-22], or primary hepatocytes that underwent gamma irradiation [17]. However, these models have certain limitations as different cell types will react differently to a given stressor [23]. Furthermore, the method of senescence induction *i.e.,* oxidative stress, gamma irradiation or overexpression of an oncogene, may contribute to variable phenotypes that may not necessarily resemble aging *in vivo* [5, 16, 23]. Thus, it is critical to verify the fidelity of *in vitro* models to tissues from aged mice. Although there still remains some uncertainty about the optimal method to induce senescence *in vitro*; it generally is agreed that oxidative stress and mitochondrial dysfunction play significant roles in the aging process [6, 11, 24, 25]. Accordingly, we have developed a method for inducing hepatic cellular senescence by using mouse hepatic Alpha Mouse Liver 12 (AML12) cells and subjecting them to repetitive oxidative stress. We also demonstrated that the senescent cells exhibited age-related molecular and metabolic changes that corresponded with liver in aged mice.

## RESULTS

### *Senescence induction and validation in AML12 cells*

AML12 cells were grown to 50% confluency and treated with 1 mM $H_2O_2$ on day 1 followed by 750 μM $H_2O_2$ for the subsequent 5 days in serum-free DMEM:F12 medium for 1 h each day as described in **Figure 1a**. After treatment, serum-free DMEM:F12 medium containing $H_2O_2$ was replaced with complete DMEM:F12 medium (containing 10% FBS, 1x ITS, 100 nM dexamethasone, and 1x penicillin and streptomycin) for a 23 h period of recovery each day. This cycle was repeated 6 times. Cells were sub-cultured/re-seeded in the ratio of 1:3 until they reached confluency >80% after approximately 3 days. As shown in **Figure 1b**, morphological effects such as cellular hypertrophy can be seen after 2 days of $H_2O_2$ treatment. After 6 days of multiple $H_2O_2$ treatments, the cells showed classical features of senescence as they were distinctly larger and showed less proliferation than untreated controls (**Figure 1b,c**) [8]. Moreover, the mRNA expression of senescence marker genes, *P53*, *P21* and *P16* were increased in the senescent AML12 cells compared to control AML12 cells (**Figure 1d**). Similarly, the expression of these genes also was increased in livers from old mice (100-108 week age) compared to those from young mice (12-20 week age) (**Figure 1e**). Furthermore, multiple $H_2O_2$ treatments increased senescence since there was increased activated β-Gal (SA β-Gal)-positive cells (**Figure 2a,b**) and γH2A.X-positive cells containing condensed chromatin in larger nuclei (**Figure 2c,d**). Taken together, these data showed that multiple $H_2O_2$ treatments markedly induced premature senescence in AML12 cells [1].

*Bioenergetic phenotype of senescent AML12 cells*

To perform the bioenergetic phenotyping of senescent AML12 cells, we used the Seahorse extracellular flux analyzer to measure the cell's glycolytic and oxidative

potential. Senescent AML12 cells showed higher oxygen consumption rate (OCR) and extracellular acidification rate (ECAR) than control cells (**Figure 3a**). Senescent AML12 cells also were more reliant on glycolysis for cellular energy than oxidative metabolism under stress conditions (**Figure 3b**). We further analysed the glycolytic potential of senescent AML12 cells and found that they had significantly higher basal glycolysis, glycolytic potential as well as glycolytic reserve capacity than control cells (**Figure 3c,d**). Furthermore, senescent AML12 cells had marked increase in basal mitochondrial activity and maximum respiratory capacity, but no change in mitochondrial ATP production (**Figure 4a,b**). Instead, those cells showed reduced coupling efficiency and increased proton leak, suggesting they had mitochondrial dysfunction, a hallmark of cellular senescence and aging. Finally, mitochondrial fuel oxidation analysis showed there were significant reductions in glucose and fatty acid flexibilities and capacities, but an enhancement of glutatmine oxidation flexibility and capacity (**Figure 4a-c)**. However, there were no significant changes in glucose, fatty acid, or glutamine oxidation dependency (**Figure 4c**). .

*Molecular phenotyping of energy sensing molecules in senescent AML12 cells*

We next analysed the activation (via phosphorylation) of several key energy-sensing proteins: AMPK, AKT, MTOR, P70S6K (MTOR target), as well as the formation of LC3B-II and P62 (autophagy-related proteins) in senescent AML12 cells by Western blotting. As a signature of senescent cells, we observed marked increase in the phosphorylation of AMPK, AKT, MTOR and P70S6K proteins in senescent AML12 cells (**Figure 5a,b**). This phosphorylation pattern was similar to the one observed in the livers of old mice (**Figure 5c,d**). Additionally, we observed a marked increase in the expression of autophagy proteins, LC3B-II and P62, under basal

conditions suggesting there was a late autophagic block in senescent AML12 cells and in livers from old mice. Likewise, we observed the accumulation of neutral lipids in senescent AML12 cells at basal conditions that was similar to the increased hepatic triglyceride content found in old mice (Figure 5e-g).

*Senescent AML12 cells create a pro-inflammatory environment and sensitize healthy AML12 cell towards pathological damage*

Senescent cells secrete senescence-associated secretory proteins (SASP) such as IL6 and IL1b, and are thought to be responsible for creating a pro-inflammatory environment to neighbouring cells during aging-associated diseases [1, 26, 27]. We found that senescent AML12 cells showed higher expression of pro-inflammatory genes *IL1b* and *IL6* (**Figure 6a**). Similarly, liver tissue from old mice showed significantly higher expressions of *IL1b* and *IL6* (**Figure 6b**). We next treated control AML12 cells with conditioned media collected from senescent AML12 cell cultures, and found that they not only increased the expression of inflammatory (*IL1b, IL6, CCL2*) and fibrosis (*IL11*) genes in normal AML12 cells but also increased the latter's sensitivity to induction of inflammatory (*IL1b, IL6, CCL2*) and fibrosis (*IL11*) genes by saturated fatty acids (palmitate 0.5 mM for 24 h) in comparison to conditioned media prepared from control AML12 cell cultures (**Figure 6c**).

## DISCUSSION

There currently is a need for developing *in vitro* methods to understand the cellular and metabolic dysregulation that occurs in the aging liver. Such a tool would not only enable better understanding of the molecular and metabolic defects associated with aging, but also could potentially help identify druggable targets to treat age-

associated chronic hepatic diseases such as fatty liver, steatohepatitis, Type 2 diabetes, hepatic fibrosis in a time- and cost-efficient manner [3, 5-7, 16, 23]. Cellular senescence and the number of senescent cells significantly increases in most tissues during aging [9, 12, 24]. Previous *in vitro* senescence models have utilized primary fibroblasts or hepatic carcinoma cells that were subjected to oxidative stress conditions or irradiation [17-23]. However, these models have limited application to the aging liver due to differences in their respective molecular and metabolic phenotypes. Since oxidative stress and mitochondrial dysfunction are considered to be critical for senescence and aging [6, 11, 24, 25], we have developed a protocol that produces these changes to induce premature cellular senescence in non-transformed AML12 hepatic cells to study hepatic aging *in vitro*.

We found that AML12 cells subjected to multiple exposures of sublethal $H_2O_2$ dosage developed premature senescence. In particular, they showed increased expression of key senescence genes such as *P52, P21*, and *P16* as well as increased numbers of SA-βGal and γH2A.X positive cells that had condensed chromatin in larger nuclei (**Figures 1 and 2**).

Senescent cells are metabolically hyperactive and display a metabolic shift consisting of marked increases in glycolysis, mitochondrial activity, and mitochondrial damage due to proton leakage [8, 27, 28]. After AML12 cells were given multiple sublethal $H_2O_2$ doses, we found they increased their cellular bioenergetics (**Figure 3a,b**) and showed greater reliance upon glycolysis under nutrient stress conditions. Subsequent analysis of the glycolysis stress test confirmed senescent AML12 cells had greater glycolytic potential and reserve than

control cells (**Figure 3c,d**). Senescent cells also had increased mitochondrial activity compared to control cells. However, this increased activity did not lead to more ATP production due to concomitant increases in basal uncoupling and proton leakage, which are hallmarks of senescent cells [1, 25, 27, 29]. These findings thus explains the reason why there is increased AMP:ATP ratio leading to the AMPK activation often found in senescent cells [1, 27, 29]. The senescent AML12 cells also produced significantly higher basal respiration and maximum respiration (**Figure 4a,b**). However, these changes were not accompanied by increases in % spare respiratory capacity and ATP production. Notably, these changes in mitochondrial function also have been reported to be present in aging liver tissue [1]. Furthermore, mitochondrial fuel oxidation analysis showed there was significantly lower fuel flexibility and less total capacity for glucose and fatty acid oxidation in the senescent AML12 cells (**Figure 4c**). These latter findings also were consistent with impairments in hepatic fatty acid oxidation and glucose intolerance that have been described in the aging liver [1, 30]. Taken together, our findings showed that the senescent AML12 cells showed many of the key changes that cause altered metabolism and mitochondrial function in the aging liver [1, 8, 27, 28, 30].

Interestingly, senescent AML12 cells showed a compensatory increase in mitochondrial glutamine oxidation (**figure 4c**). Glutamine activates several hepatic metabolic pathways such as the activation of PEPCK and the phosphorylation p70S6K, the latter of which inhibits autophagic proteolysis to induce cell swelling [31, 32]. Furthermore, glutamine oxidation facilitates mTOR activation by leucine, an activator of glutaminolysis, to regulate cell growth and autophagy [33]. In this connection, senescent AML12 cells showed activated MTOR signaling and

increased p70S6K phosphorylation which likely inhibited autophagy (**Figure 5a,b**). Our findings were consistent with the observation that autophagy impairment associated with lysosomal and mitochondrial dysfunction is an important characteristic of oxidative stress-induced senescence [35]. On the other hand, several studies have suggested there is either activation of autophagy or no apparent change in autophagy during senescence [28, 34]. These differences suggest that may be cell-specific changes in autophagy during senescence. Nonetheless, it appears that in the liver, autophagy likely decreases with aging and may be involved in many age-related diseases such as NAFLD and Type 2 DM [1, 3, 11, 12, 36]. In this connection, we found that both senescent AML12 cells and livers from aged mice showed late autophagy block associated with increased intracellular fat content (**Figure 5a-g**).

AMPK is a glucose and cellular energy sensor that is activated during states of energy depletion. In the liver, it is able to sense increased AMP:ATP and ADP:ATP concentration ratios, and activates compensatory responses such as increasing fatty acid oxidation, mitochondrial biogenesis, and glucose uptake, as well as inhibiting fatty acid synthesis [37, 38]. AMPK activation also induces cell cycle arrest and senescence by directly phosphorylating P53 on multiple sites [39]. In contrast to AMPK, which senses energy depletion and activates catabolic pathways, MTOR senses the fed state and activates anabolic pathways during cell growth and proliferation. Thus, AMPK and MTOR often have opposing roles in metabolic tissues of mammals [40]. However, the reciprocal actions of AMP and MTOR in maintaining metabolic homeostatic becomes impaired during senescence, and leads to concurrent activation of both MTOR and AMPK. This dysregulation also is found in

the aging liver [1, 27, 28]. In this connection, we found that AMPK and MTOR both were activated in senescent AML12 cells (**Figure 5**), suggesting that energy sensing had become dysregulated as evident by impaired oxidative phosphorylation (**Figure 4a,b**) and compensatory increase in glycolysis (**Figure 3c,d**). Although no change or inhibition of MTOR signaling has been reported previously for the liver during aging [41, 42], it is noteworthy that genetic or pharmacological inhibition of MTOR, or its activation by calorie restriction followed by autophagy, increases life span and decreases aging-related changes in tissues [29, 43-47].

SASP is an energy-dependent process in which senescent cells secrete high levels of inflammatory cytokines, immune modulators, growth factors, and proteases [7, 8, 28, 48, 49]. IL6 and IL1β are major secretory interleukins present in SASP, and are associated with the pro-inflammatory environment that occurs during aging [1, 3, 8, 50]. In this connection, we observed a marked increase in glycolysis in senescent AML12 cells (**Figure 3c,d**) that was accompanied by increased expression of IL6 and IL1β. Similar findings also were observed in livers from aged mice (**Figure 6a,b**). Interestingly, when we incubated healthy AML12 cells with conditional media collected from senescent AML12 cells , they became more sensitive to the inflammatory response caused by the saturated fatty acid, palmitate (**Figure 6c**). Our findings were consistent with previous reports suggesting that SASP plays an important role in generating a pro-inflammatory environment during aging and age-related metabolic diseases.

In conclusion, we have developed a protocol to generate senescent AML12 hepatic cells that faithfully recapitulate many of the features of senescence found in

livers from aged mice. In particular, the senescent AML12 cells expressed many of the key cellular markers of senescence, and exhibited similar altered mitochondrial metabolism and molecular signaling as the livers in aged mice. Thus, these cells should be an useful tool to study hepatic aging *in vitro* which previously was delimited by the need to use senescent fibroblasts or hepatic cancer cells. Furthermore, the senescent AML12 cells created a pro-inflammatory environment that rendered neighbouring hepatic cells more susceptible to saturated fatty acid-induced toxicity. The latter often occurs in NAFLD during the progression from hepatosteatosis to non-alcoholic steatohepatitis (NASH). Thus, it is possible that SASPs may be important for the pathological transition to NASH. In this regard, senescent AML12 cells would be useful to identify SASPs and understand their roles in causing inflammation in hepatic cells. These cells also could be useful for understanding the pathological molecular and metabolic changes that occur in age-related chronic hepatic diseases such as NASH, hepatic cirrhosis, and HCC, as well as for screening nutraceuticals and pharmaceuticals that might be useful to treat the pathological features associated with aging and senescence, and their associated metabolic conditions [4, 16, 17, 48, 49, 51, 52].

## METHODS

### *Senescence induction in normal mouse AML12 cells and analysis of cell replication*

The AML12 (alpha mouse liver 12) cells were purchased from ATCC, USA (ATCC® CRL-2254™) and maintained as described in the standard protocol (https://www.atcc.org/Products/All/CRL-2254.aspx#culturemethod). $4x10_6$ AML12 cells were seeded in a T175 cell culture flask for senescence induction. 30% (9.77

M) hydrogen peroxide ($H_2O_2$) was used for senescence induction. At day 1, cells were treated with 1 mM $H_2O_2$ for 1 h in serum-free medium followed by incubation in complete DMEM:F12 medium (containing 10% FBS, 1x ITS, 100 nM dexamethasone, and 1x penicillin and streptomycin) for recovery for 23 h. from day 2 to day 6, 750 μM $H_2O_2$ for 1 h in serum-free medium followed by 23 h recovery was used. Morphological changes should be visualized from day 3 of $H_2O_2$ treatment (**figure 1b**). At day 7, $0.3x10_6$ control and senescent AML12 cells were seeded in each well of 6-well plate for cell replication analysis and counted (using Countess™ II Automated Cell Counter, ThermoFisher) at every other day for three days as shown in **figure 1c**.

*Senescence activated secretory phenotype (SASP)-induced palmitate toxicity*

AML12 senescence was induced as described above and after day 7 AML12 complete media was replaced with basal media (DMEM:F12) containing only 1x penicillin and streptomycin for 24 h. The next day, this conditional media was collected from control and senescent AML12 cells and put on new control AML12 cells seeded in other 6-well plates for 24 h. Palmitate was used at 0.5 mM concentration in 0.5% BSA supplemented (in a pathological FA:BSA ratio 6:1) in control media as well as senescent conditional media was used to represent pathological fatty acids concentration in serum [53]. Equivalent BSA was used in appropriate controls.

*Animal experiments*

12-20 weeks age male C57BL6/J mice (consider young), whereas 100-108 weeks age male C57BL6/J mice (consider old) were purchased from Jacksons Laboratory

USA (Stock: 000664) and used in this study. Animals were housed in hanging polycarbonate cages under a 12 h light/12 h dark cycle at 23 °C with food and water available *ad libitum*. All cages contained shelters and nesting material. 6 h fasted mice euthanized and liver was collected and snap frozen in liquid nitrogen for subsequent analysis. All mice were maintained according to the Guide for the Care and Use of Laboratory Animals (National Institutes of Health publication 1.0.0; revised 2011), and experiments were approved by SingHealth Institutional Animal Care and Use Committee.

*mRNA expression analysis by reverse transcription-quantitative PCR*

Total RNA isolation from cultured cells and liver tissue was performed using InviTrap Spin Universal RNA kit (Stratec Biomedical, Birkenfeld, Germany), and RT-qPCR was performed as described previously [54] using QuantiTect SYBR Green PCR kit and KiCqStart SYBR Green optimized primers from Sigma-Aldrich (KSPQ12012).

*Protein extraction and expression analysis by Western blotting*

Cultured cells or 50 mg of liver tissues were lysed using CelLytic M mammalian cell lysis/extraction reagent (C2978, Sigma-Aldrich). An aliquot was removed, and protein concentrations were measured using the BCA kit (Bio-Rad). Western blotting was performed using a standard protocol, as described previously [55]. Primary antibodies at dilution 1:500 for phospho-AMPK-alpha (T172) (CST: 2535S), phospho-AKT (S473) (CST: 4058S), phospho-mTOR (S2448) (CST: 5536S), phospho-p70S6K (S371) (CST: 9208S), 1:5000 for LC3B-II (CST: 2775S), GAPDH (CST: 2118L), and 1:1000 for p62 (CST: 5114S) were used. Western blot images

were captured on the Gel-Doc system (Bio-Rad), and densitometry analysis was performed using ImageJ software (National Institutes of Health). The integrated density of target protein was normalized with the GAPDH; the mean was plotted in graphs.

*Immunofluorescence analysis for γH2A.X*

Cells were cultured in 4-well chambered slides, fixed in 4% paraformaldehyde and incubated in 1:200 diluted γH2A.X antibody (CST: 9718) overnight at 4 $^{o}$C after blocking as described previously [56]. 1:200 Alexa Fluor 488 (Molecular Probes, ThermoFisher) was used to collect signals. Cells were counter-stained with 5 μM Hoechst 33342 (Abcam: ab228551) for 5 min and mounted using VECTASHIELD® Antifade Mounting Medium H-1000 (Vector Laboratories), and visualized under 40x magnification using Zeiss LSM confocal microscope. Five images were clicked randomly using ZEN 2 (blue edition) software and quantification of green fluorescence was normalized with blue using ImageJ software (National Institutes of Health) and plotted as a graph.

*Senescent associated β-Gal staining in AML12 cells*

Cellular Senescence Assay kit (Merck Millipore: KAA002) was used to detect senescent AML12 by SA β-Gal staining as per the manufacturer's protocol. X-Gal staining was performed overnight at 37 $^{o}$C and crystals were visualized under the microscope at 10x magnification. Five images were captured randomly using Olympus inverted microscope and cells were counted for SA β-Gal$^{+}$ Cells, and shown as percent positive cells.

*Seahorse extracellular flux analysis for bioenergetic phenotyping, mitostress test, glycolytic stress test and mitochondrial fuel oxidation analysis*

Seahorse extracellular flux analyser XFe96 (Agilent) was used for bioenergetic phenotyping, mitostress test, glycolytic stress test and mitochondrial fuel oxidation analysis, and Seahorse Wave Desktop software was used for report generation and data analysis, and GraphPad PRISM 8 was used for statistical analysis and data presentation.

Bioenergetic phenotyping: Agilent Seahorse XF Cell Energy Phenotype Test kit was used with Agilent Seahorse XFe96 Extracellular Flux Analyzer that rapidly measures mitochondrial respiration and glycolysis under baseline and stressed conditions, to reveal the three key parameters of cell energy metabolism: Baseline Phenotype, Stressed Phenotype, and Metabolic Potential (https://www.agilent.com/cs/library/usermanuals/public/XF_Cell_Energy_Phenotype_Test_Kit_User_Guide.pdf). Simultaneous acute injections of mitochondrial inhibitors oligomycin and FCCP reveals live cell's metabolic potential under stress. Oligomycin (1 μM) inhibits ATP production by the mitochondria, and causes a compensatory increase in the rate of glycolysis as the cells attempt to meet their energy demands via the glycolytic pathway. Whereas, FCCP (1 μM) depolarizes the mitochondrial membrane, and drives oxygen consumption rates higher as the mitochondria attempt to restore the mitochondrial membrane potential.

Glycolysis stress test: Agilent Seahorse XF Glycolysis Stress Test Kit was used as per the standard protocol by Agilent Seahorse (https://www.agilent.com/en-us/agilent404?s=www.agilent.com/cs/library/usermanuals/public/XF_Glycolysis_Str

ess_Test_Kit_User_Guide.pdf). Glucose conversion to lactate (Glycolysis) results in net production and extrusion of protons into the extracellular medium (acidification). As glycolysis occurs, the resulting acidification of the medium surrounding the cells is measured directly by the analyzer and reported as the Extracellular Acidification Rate (ECAR).

To understand the complete glycolytic potential of the cell, ECAR of cells was measured (three times) before and after sequential injections of three different compounds, glucose (10 mM), oligomycin (1 μM) and 2-Deoxy-D-glucose (2-DG; 100 mM) sequentially.

Mito stress test: Agilent Seahorse XF Mito Stress Test Kit was used as per the standard protocol by Agilent Seahorse (https://www.agilent.com/cs/library/usermanuals/public/XF_Cell_Mito_Stress_Test_Kit_User_Guide.pdf). This test measures key parameters of mitochondrial function by directly measuring the oxygen consumption rate (OCR) of cells. Oligomycin (1 μM; inhibits ATP synthase) was injected first following basal OCR measurements. The second injection of FCCP (1 μM; a uncoupling agent that collapses the proton gradient and disrupts the mitochondrial membrane potential) followed by the third injection which was a mixture of rotenone (1 μM; a complex I inhibitor) and antimycin A (1 μM; a complex III inhibitor).

Mito fuel flex test: Agilent Seahorse XF Mito Fuel Flex Test Kit was used as per the standard protocol by Agilent Seahorse (https://www.agilent.com/cs/library/usermanuals/public/XF_Mito_Fuel_Flex_Test_Kit_User_Guide%20old.pdf). This test measures the dependency, capacity, and

flexibility of cells to oxidize three mitochondrial fuels in real-time in living cells: Glucose (pyruvate), Glutamine (glutamate) and Long-chain fatty acids. This test determines the rate of oxidation of each of these fuels by measuring OCR of cells in the presence or absence of fuel pathway inhibitors. UK5099 (2 μM; glucose oxidation pathway inhibitor) that blocks the mitochondrial pyruvate carrier (MPC); BPTES (3 μM; glutamine oxidation pathway inhibitor) that allosterically inhibits glutaminase (GLS1); and Etomoxir (4 μM; long chain fatty acid oxidation inhibitor) that inhibits carnitine palmitoyl-transferase 1A (CPT1A), a critical enzyme of mitochondrial beta-oxidation.

The data later represented as fuel oxidation dependency, flexibility and total capacity. 'Dependency' indicates the fuel oxidation at basal in control or senescence cells. Inhibiting the two alternative pathways followed by the pathway of interest enables the calculation of cells' mitochondrial 'capacity' to meet energy demand. 'Flexibility' (that is calculated by subtracting the dependency from the capacity for the target fuel oxidation pathway) indicates the cells' mitochondria can compensate for the inhibited pathway by using other pathways to fuel mitochondrial respiration. The presence of dependency and the absence of flexibility demonstrates that the mitochondria require that fuel pathway to maintain basal OCR.

*Immunofluorescence imaging of intracellular lipids using BODIPY™ 493/503*

Control and senescent aml12 cells were seeded in 24-well plate at 7th day of the protocol, and cultured for 24 h. Cells were rinsed with 1x PBS and stained with BODIPY™ 493/503 (D3922; Molecular Probes, ThermoFisher Scientific ) at 1:1000 dilution for 15 min. Cells were then rinsed with 1xPBS containing Hoechst 33342 (Sigma) to counter stain nucleus for 5 min. After rinse, cells were kept in 1x HBSS

for imaging. Leica fluorescent microscope was used at 10x magnification for visualization and LAS X imaging software was used for image capture.

*Liver triglycerides measurements in young and old mice*

Liver triglyceride was measured using triglyceride colorimetric assay kit (Cayman Chemical) as per the manufacturer's protocol.

*Statistical methods*

The data was calculated and presented as Mean±SD. The parametric unpaired t-test was use to compute significance between two groups, whereas Two-way ANOVA followed by Tukey's multiple comparisons test was used to compute significance between more than two groups. GraphPad PRSIM 8 was used for statistical analysis and data representation.

ACKNOWLEDGMENTS

The authors would like to thank Ms. Jia Pei and Mr. Kiraely Adam Wong Zongren for their assistance and help during this study.

AUTHOR CONTRIBUTIONS

Conceived and designed the experiments: BKS MT. Performed the experiments: BKS MT RS KT. Analyzed the data: BKS MT JZ. Contributed reagents/materials /analysis tools: PMY BKS MT JZ. Wrote the manuscript: BKS MT PMY.

CONFLICTS OF INTEREST

The authors declare no conflict of interest.

FUNDING

This research was funded by the Ministry of Health (MOH), and National Medical Research Council (NMRC), Singapore, grant number NMRC/OFYIRG/0002/2016 and MOH-000319 (MOH-OFIRG19may-0002) to BKS; NMRC/OFYIRG/077/2018 to MT; and CSAI19may-0002 to PMY; Duke-NUS Medical School and Estate of Tan Sri Khoo Teck Puat Khoo Pilot Award (Collaborative) Duke-NUS-KP(Coll)/2018/0007A to JZ.

REFERENCES

1. Hunt NJ, Kang SWS, Lockwood GP, Le Couteur DG, Cogger VC. Hallmarks of Aging in the Liver. Comput Struct Biotechnol J. 2019; 17: 1151-61.
2. Jiang JX, Fish SR, Tomilov A, Li Y, Fan W, Dehnad A, Gae D, Das S, Mozes G, Charville GW, Ramsey J, Cortopassi G, Torok NJ. Non-phagocytic Activation of NOX2 is Implicated in Progressive Non-alcoholic Steatohepatitis During Aging. Hepatology. 2020.
3. Kim IH, Kisseleva T, Brenner DA. Aging and liver disease. Curr Opin Gastroenterol. 2015; 31: 184-91.
4. Papatheodoridi AM, Chrysavgis L, Koutsilieris M, Chatzigeorgiou A. The Role of Senescence in the Development of Nonalcoholic Fatty Liver Disease and Progression to Nonalcoholic Steatohepatitis. Hepatology. 2020; 71: 363-74.
5. Campisi J, Kapahi P, Lithgow GJ, Melov S, Newman JC, Verdin E. From discoveries in ageing research to therapeutics for healthy ageing. Nature. 2019; 571: 183-92.
6. Ferrucci L, Gonzalez-Freire M, Fabbri E, Simonsick E, Tanaka T, Moore Z, Salimi S, Sierra F, de Cabo R. Measuring biological aging in humans: A quest. Aging Cell. 2020; 19: e13080.
7. Gorgoulis V, Adams PD, Alimonti A, Bennett DC, Bischof O, Bishop C, Campisi J, Collado M, Evangelou K, Ferbeyre G, Gil J, Hara E, Krizhanovsky V, et al. Cellular Senescence: Defining a Path Forward. Cell. 2019; 179: 813-27.
8. Hernandez-Segura A, Nehme J, Demaria M. Hallmarks of Cellular Senescence. Trends Cell Biol. 2018; 28: 436-53.
9. Schmeer C, Kretz A, Wengerodt D, Stojiljkovic M, Witte OW. Dissecting Aging and Senescence-Current Concepts and Open Lessons. Cells. 2019; 8.
10. Stahl EC, Haschak MJ, Popovic B, Brown BN. Macrophages in the Aging Liver and Age-Related Liver Disease. Front Immunol. 2018; 9: 2795.
11. Baker BM, Haynes CM. Mitochondrial protein quality control during biogenesis and aging. Trends Biochem Sci. 2011; 36: 254-61.
12. Belikov AV. Age-related diseases as vicious cycles. Ageing Res Rev. 2019; 49: 11-26.

13. Palmer AK, Gustafson B, Kirkland JL, Smith U. Cellular senescence: at the nexus between ageing and diabetes. Diabetologia. 2019; 62: 1835-41.
14. Palmer AK, Xu M, Zhu Y, Pirtskhalava T, Weivoda MM, Hachfeld CM, Prata LG, van Dijk TH, Verkade E, Casaclang-Verzosa G, Johnson KO, Cubro H, Doornebal EJ, et al. Targeting senescent cells alleviates obesity-induced metabolic dysfunction. Aging Cell. 2019; 18: e12950.
15. Patil P, Dong Q, Wang D, Chang J, Wiley C, Demaria M, Lee J, Kang J, Niedernhofer LJ, Robbins PD, Sowa G, Campisi J, Zhou D, et al. Systemic clearance of p16(INK4a) -positive senescent cells mitigates age-associated intervertebral disc degeneration. Aging Cell. 2019; 18: e12927.
16. Thoppil H, Riabowol K. Senolytics: A Translational Bridge Between Cellular Senescence and Organismal Aging. Front Cell Dev Biol. 2019; 7: 367.
17. Ogrodnik M, Miwa S, Tchkonia T, Tiniakos D, Wilson CL, Lahat A, Day CP, Burt A, Palmer A, Anstee QM, Grellscheid SN, Hoeijmakers JHJ, Barnhoorn S, et al. Cellular senescence drives age-dependent hepatic steatosis. Nat Commun. 2017; 8: 15691.
18. Chen JH, Ozanne SE, Hales CN. Methods of cellular senescence induction using oxidative stress. Methods Mol Biol. 2007; 371: 179-89.
19. Carnero A. Markers of cellular senescence. Methods Mol Biol. 2013; 965: 63-81.
20. Chen H, Li Y, Tollefsbol TO. Cell senescence culturing methods. Methods Mol Biol. 2013; 1048: 1-10.
21. Aravinthan A, Shannon N, Heaney J, Hoare M, Marshall A, Alexander GJ. The senescent hepatocyte gene signature in chronic liver disease. Exp Gerontol. 2014; 60: 37-45.
22. Pan C, Lang H, Zhang T, Wang R, Lin X, Shi P, Zhao F, Pang X. Conditioned medium derived from human amniotic stem cells delays H2O2induced premature senescence in human dermal fibroblasts. Int J Mol Med. 2019; 44: 1629-40.
23. Childs BG, Gluscevic M, Baker DJ, Laberge RM, Marquess D, Dananberg J, van Deursen JM. Senescent cells: an emerging target for diseases of ageing. Nat Rev Drug Discov. 2017; 16: 718-35.
24. Liguori I, Russo G, Curcio F, Bulli G, Aran L, Della-Morte D, Gargiulo G, Testa G, Cacciatore F, Bonaduce D, Abete P. Oxidative stress, aging, and diseases. Clin Interv Aging. 2018; 13: 757-72.
25. Panel M, Ghaleh B, Morin D. Mitochondria and aging: A role for the mitochondrial transition pore? Aging Cell. 2018; 17: e12793.
26. Coppe JP, Patil CK, Rodier F, Sun Y, Munoz DP, Goldstein J, Nelson PS, Desprez PY, Campisi J. Senescence-associated secretory phenotypes reveal cell-nonautonomous functions of oncogenic RAS and the p53 tumor suppressor. PLoS Biol. 2008; 6: 2853-68.
27. Sabbatinelli J, Prattichizzo F, Olivieri F, Procopio AD, Rippo MR, Giuliani A. Where Metabolism Meets Senescence: Focus on Endothelial Cells. Front Physiol. 2019; 10: 1523.
28. Wiley CD, Campisi J. From Ancient Pathways to Aging Cells-Connecting Metabolism and Cellular Senescence. Cell Metab. 2016; 23: 1013-21.
29. Stead ER, Castillo-Quan JI, Miguel VEM, Lujan C, Ketteler R, Kinghorn KJ, Bjedov I. Agephagy - Adapting Autophagy for Health During Aging. Front Cell Dev Biol. 2019; 7: 308.
30. Gong Z, Tas E, Yakar S, Muzumdar R. Hepatic lipid metabolism and non-alcoholic fatty liver disease in aging. Mol Cell Endocrinol. 2017; 455: 115-30.

31. Meynial-Denis D. Glutamine metabolism in advanced age. Nutr Rev. 2016; 74: 225-36.
32. Haussinger D, Schliess F. Glutamine metabolism and signaling in the liver. Front Biosci. 2007; 12: 371-91.
33. Duran RV, Oppliger W, Robitaille AM, Heiserich L, Skendaj R, Gottlieb E, Hall MN. Glutaminolysis activates Rag-mTORC1 signaling. Mol Cell. 2012; 47: 349-58.
34. Cho S, Hwang ES. Status of mTOR activity may phenotypically differentiate senescence and quiescence. Mol Cells. 2012; 33: 597-604.
35. Tai H, Wang Z, Gong H, Han X, Zhou J, Wang X, Wei X, Ding Y, Huang N, Qin J, Zhang J, Wang S, Gao F, et al. Autophagy impairment with lysosomal and mitochondrial dysfunction is an important characteristic of oxidative stress-induced senescence. Autophagy. 2017; 13: 99-113.
36. Amir M, Czaja MJ. Autophagy in nonalcoholic steatohepatitis. Expert Rev Gastroenterol Hepatol. 2011; 5: 159-66.
37. Hardie DG, Ross FA, Hawley SA. AMPK: a nutrient and energy sensor that maintains energy homeostasis. Nat Rev Mol Cell Biol. 2012; 13: 251-62.
38. Lin SC, Hardie DG. AMPK: Sensing Glucose as well as Cellular Energy Status. Cell Metab. 2018; 27: 299-313.
39. Jones RG, Plas DR, Kubek S, Buzzai M, Mu J, Xu Y, Birnbaum MJ, Thompson CB. AMP-activated protein kinase induces a p53-dependent metabolic checkpoint. Mol Cell. 2005; 18: 283-93.
40. Gwinn DM, Shaw RJ. (2010). AMPK Control of mTOR Signaling and Growth. In: Tamanoi F and Hall MN, eds. The Enzymes: Elsevier BV), pp. 49-75.
41. Baar EL, Carbajal KA, Ong IM, Lamming DW. Sex- and tissue-specific changes in mTOR signaling with age in C57BL/6J mice. Aging Cell. 2016; 15: 155-66.
42. Leontieva OV, Paszkiewicz GM, Blagosklonny MV. Fasting levels of hepatic p-S6 are increased in old mice. Cell Cycle. 2014; 13: 2656-9.
43. Harrison DE, Strong R, Sharp ZD, Nelson JF, Astle CM, Flurkey K, Nadon NL, Wilkinson JE, Frenkel K, Carter CS, Pahor M, Javors MA, Fernandez E, et al. Rapamycin fed late in life extends lifespan in genetically heterogeneous mice. Nature. 2009; 460: 392-5.
44. Hansen M, Kapahi B. (2010). TOR Signaling and Aging. In: Tamanoi F and Hall MN, eds. The Enzymes: Elsevier BV), pp. 279-99.
45. Savini M, Zhao Q, Wang MC. Lysosomes: Signaling Hubs for Metabolic Sensing and Longevity. Trends Cell Biol. 2019; 29: 876-87.
46. Papadopoli D, Boulay K, Kazak L, Pollak M, Mallette F, Topisirovic I, Hulea L. mTOR as a central regulator of lifespan and aging. F1000Res. 2019; 8.
47. Weichhart T. mTOR as Regulator of Lifespan, Aging, and Cellular Senescence: A Mini-Review. Gerontology. 2018; 64: 127-34.
48. Herranz N, Gil J. Mechanisms and functions of cellular senescence. J Clin Invest. 2018; 128: 1238-46.
49. Tchkonia T, Zhu Y, van Deursen J, Campisi J, Kirkland JL. Cellular senescence and the senescent secretory phenotype: therapeutic opportunities. J Clin Invest. 2013; 123: 966-72.
50. Chen H, Ruiz PD, McKimpson WM, Novikov L, Kitsis RN, Gamble MJ. MacroH2A1 and ATM Play Opposing Roles in Paracrine Senescence and the Senescence-Associated Secretory Phenotype. Mol Cell. 2015; 59: 719-31.
51. Aravinthan AD, Alexander GJM. Senescence in chronic liver disease: Is the future in aging? J Hepatol. 2016; 65: 825-34.

52. Kim EC, Kim JR. Senotherapeutics: emerging strategy for healthy aging and age-related disease. BMB Rep. 2019; 52: 47-55.
53. Alsabeeh N, Chausse B, Kakimoto PA, Kowaltowski AJ, Shirihai O. Cell culture models of fatty acid overload: Problems and solutions. Biochim Biophys Acta Mol Cell Biol Lipids. 2018; 1863: 143-51.
54. Zhou J, Chong SY, Lim A, Singh BK, Sinha RA, Salmon AB, Yen PM. Changes in macroautophagy, chaperone-mediated autophagy, and mitochondrial metabolism in murine skeletal and cardiac muscle during aging. Aging (Albany NY). 2017; 9: 583-99.
55. Singh BK, Sinha RA, Zhou J, Tripathi M, Ohba K, Wang ME, Astapova I, Ghosh S, Hollenberg AN, Gauthier K, Yen PM. Hepatic FOXO1 Target Genes Are Co-regulated by Thyroid Hormone via RICTOR Protein Deacetylation and MTORC2-AKT Protein Inhibition. J Biol Chem. 2016; 291: 198-214.
56. Singh BK, Sinha RA, Tripathi M, Mendoza A, Ohba K, Sy JAC, Xie SY, Zhou J, Ho JP, Chang CY, Wu Y, Giguere V, Bay BH, et al. Thyroid hormone receptor and ERRalpha coordinately regulate mitochondrial fission, mitophagy, biogenesis, and function. Sci Signal. 2018; 11.

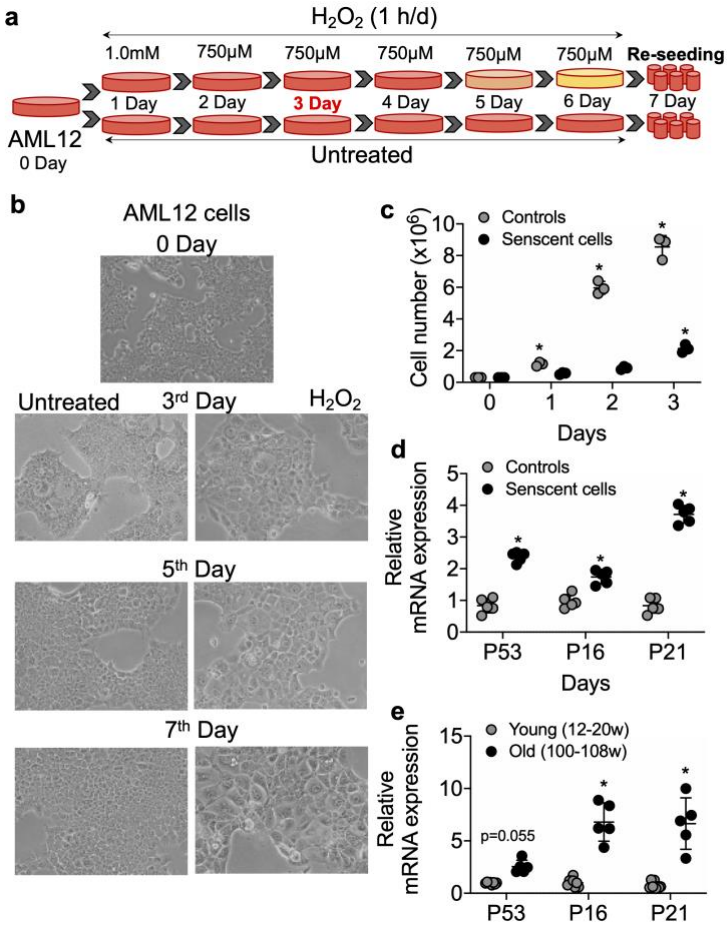


Figure 1

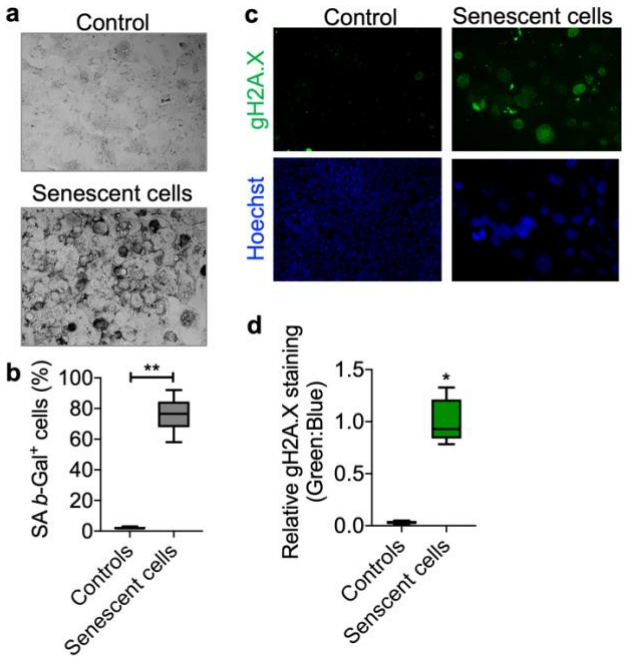


Figure 2

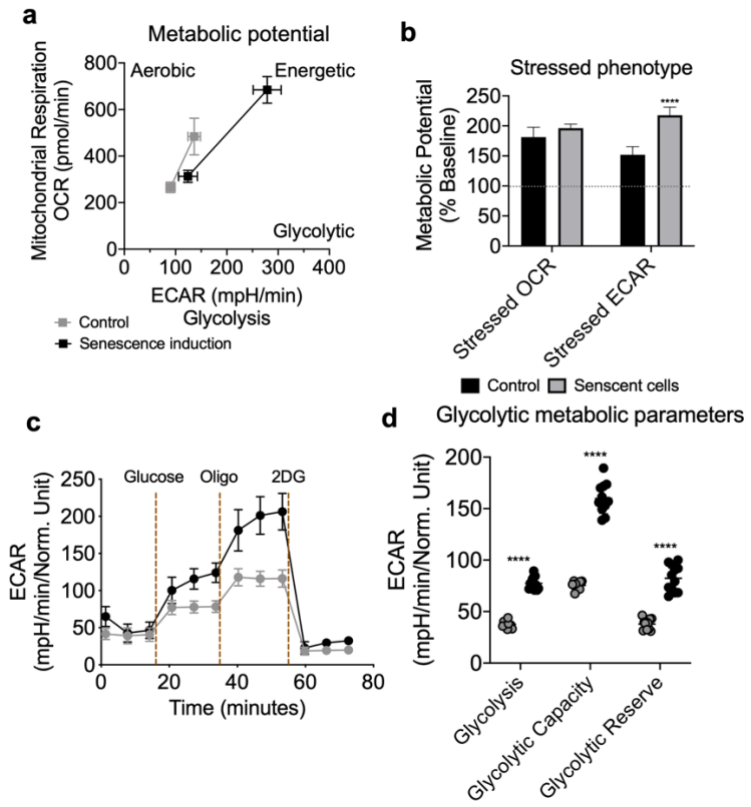


Figure 3

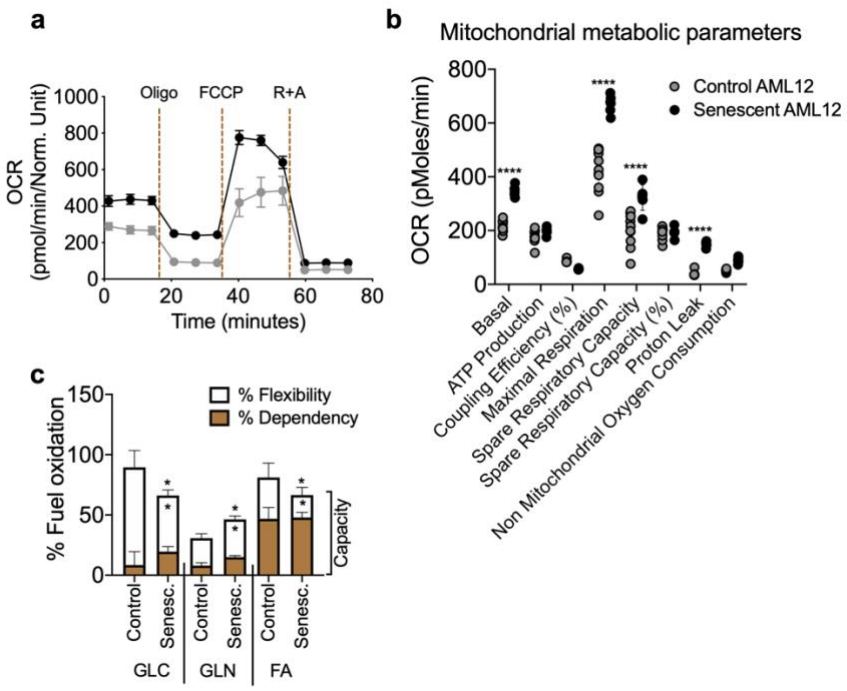


Figure 4

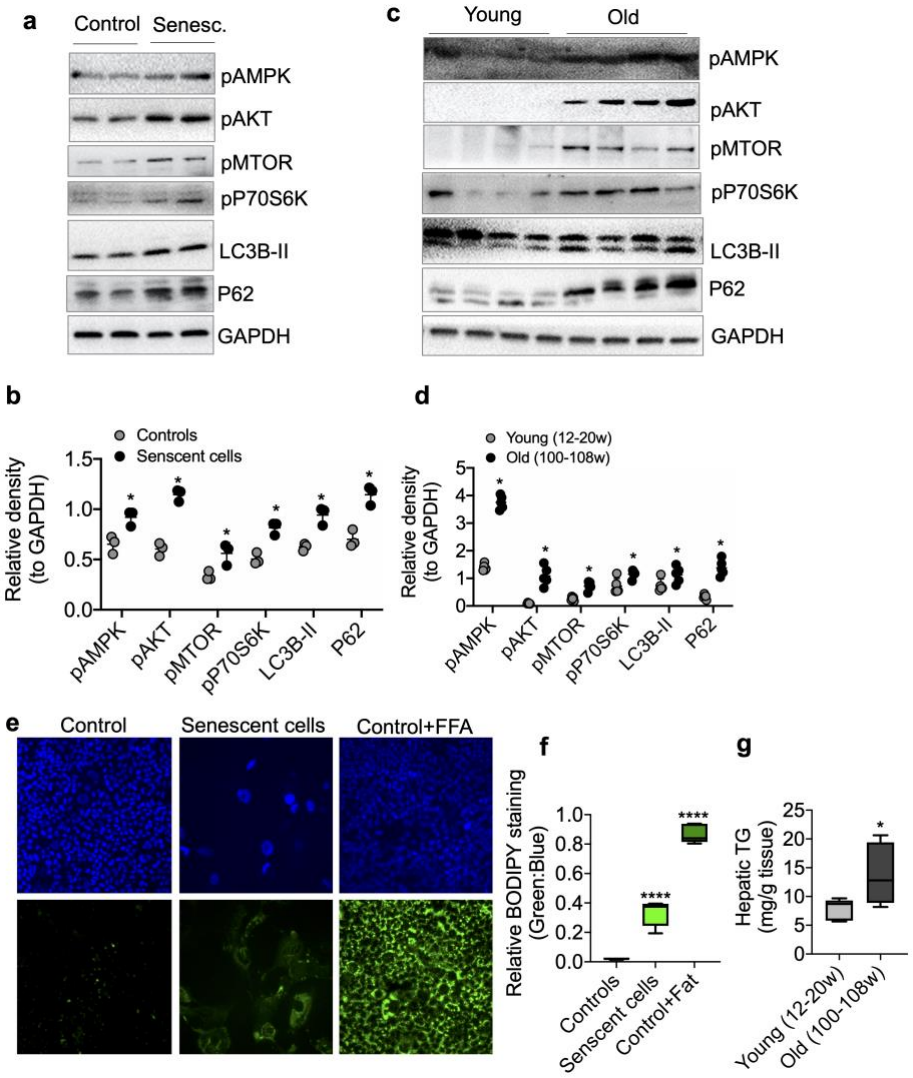
a
Control
Senesc.
pAMPK
pAKT
pMTOR
pP70S6K
LC3B-II
P62
GAPDH
c
Young
Old
pAMPK
pAKT
pMTOR
pP70S6K
LC3B-II
P62
GAPDH
b
Controls
Senscent cells
Relative density (to GAPDH)
pAMPK
pAKT
pMTOR
pP70S6K
LC3B-II
P62
d
Young (12-20w)
Old (100-108w)
Relative density (to GAPDH)
e
Control
Senescent cells
Control+FFA
f
Relative BODIPY staining (Green:Blue)
Controls
Senscent cells
Control+Fat
g
Hepatic TG (mg/g tissue)
Young (12-20w)
Old (100-108w)

Figure 5

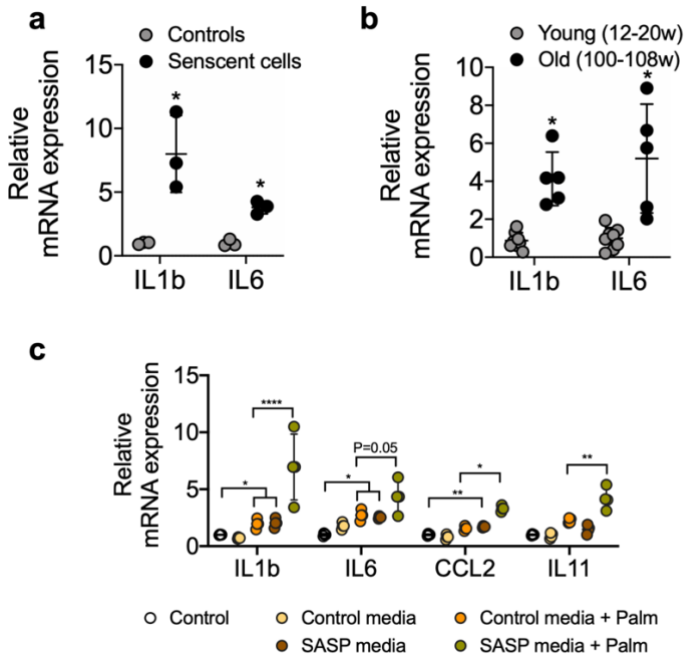


Figure 6

FIGURE LEGENDS

Figure 1. **Senescence induction in mice normal hepatic cells AML12**. (**a)** Schematic representation of experimental strategy for the senescence induction. $4x10_6$ Cells were seeded at day 0 in T175 cell culture flask. Next day (day 1) cells were treated with 1.0 mM $H_2O_2$ followed by 750 μM for the subsequent 5 days. Cells can be sub-cultured at 1:3 ratio at day 3 if required. At day 7, cells were re-seeded for experiments as required. (**b**) Visualization of senescence induction in mice AML12 cells during $H_2O_2$ treatments from day 3, day 5 and day 7 before re-seeding. The images are taken randomly at 10x magnification. (**c**) $0.3x10_6$ control and senescent AML12 cells were seeded in each well of the 6-well plate. Cells were trypsinized at indicated days and counted by an automated cell counter. (**d and e**) RT-qPCR analysis of senescence genes in AML12 cells (d) and liver tissues from young and old mice (e). * Statistical differences were calculated significant as $p<0.05$.

Figure 2. **Senescence validation by SA β-Gal and γH2A.X staining**. After senescence induction at day 7, cells were re-seeded in 4-chambered slides and next day SA β-Gal (**a**) and γH2A.X (**b**) staining were performed. Cells were counted manually for analysing SA β-Gal+ cells over total cells and presented as percent positive cells (**c**). Cells were counter-stained with Hoechst 33324 for immunofluorescence imaging and relative γH2A.X signals were analysed over Hoechst 33324 signals (**d**). Statistical differences were calculated significant as *$p<0.05$ and **$p<0.001$.

Figure 3. **Seahorse extracellular flux analysis for metabolic potential and glycolytic flux in senescent AML12 cells**. Agilent Seahorse XF Cell Energy Phenotype Test kit was used with Agilent Seahorse XFe96 Extracellular Flux Analyzer to analyse control and senescent AML12 cell's metabolic potential (**a**) and stressed phenotype (**b**). Oxygen consumption rate (OCR) represents mitochondrial respiration while the extracellular acidification rate (ECAR) represents glycolytic potential under basal and stressed conditions (as described in Methods) (**a**). Percent change in mitochondrial oxidative phenotype (OCR) and glycolytic phenotype (ECAR) under stress over basal (100%) conditions (**b**). Agilent Seahorse XF Glycolysis Stress Test kit was used with Agilent Seahorse XFe96 Extracellular Flux Analyzer to analyse control and senescent AML12 cell's glycolytic flux and reserve capacity (**c**). Glycolytic metabolic parameters were calculated as described in the Methods (**d**). All the parameters presented in the panel b and d were calculated using Seahorse Wave Desktop software. Statistical differences were calculated significant as ****$p<0.0001$.

Figure 4. **Seahorse extracellular flux analysis for mitochondrial metabolic parameters and fuel oxidation in senescent AML12 cells**. Agilent Seahorse XF Mito Stress Test kit was used with Agilent Seahorse XFe96 Extracellular Flux Analyzer to analyse control and senescent AML12 cell's mitochondrial metabolic potential (**a** and **b**). (**c**) Agilent Seahorse XF Mito Fuel Flex kit was used with Agilent Seahorse XFe96 Extracellular Flux Analyzer to analyse control and senescent AML12 cell's mitochondrial fuel (glucose, glutamine and fatty acids) oxidation. All the parameters presented in the panel b and c were calculated using Seahorse Wave Desktop software. Statistical differences were calculated significant as *$p<0.05$ and ****$p<0.0001$.

Figure 5. **Molecular analysis of energy sensing pathways in senescent AML12 cells and liver tissues from young and old mice**. (**a)** Western blot analysis of energy sensing and autophagic proteins including GAPDH in control and senescent AML12 cells. **(b**) Relative densitometric values of Western blots were calculated using ImageJ (NIH) software and normalized to GAPDH (n=3). (**c**) Western blot analysis of energy sensing and autophagic proteins including GAPDH in liver tissue from young and old mice. **(d**) Relative densitometric values of Western blots were calculated using ImageJ (NIH) software and normalized to GAPDH (n=5). (**e**) Immunofluorescence analysis of neutral lipids accumulation (fat droplets) in control and senescent AML12 cells using BODIPY stain. Images were taken at 10x magnification. Control cells were treated overnight with 0.75 mM fatty acids Oleic Acid : Palmitic Acid (2:1) as positive control. **(f**) Relative BODIPY fluorescence was calculated over Hoechst 33342 fluorescence using ImageJ software (NIH). (**g**) Hepatic triglyceride measurement was performed in the liver tissues from young and

old mice. Statistical differences were calculated significant as *p<0.05 and ****p<0.0001.

Figure 6. **RT-qPCR analysis of SASP-related proinflammatory genes in senescent AML12 cells and liver tissues from young and old mice**. RT-qPCR analysis of SASP-related proinflammatory genes in senescent AML12 cells (**a**) and liver tissues from young and old mice (**b**). (**c**) RT-qPCR analysis of inflammatory interleukins, chemokine CCL2 and fibrotic IL11 genes in control AML12 cells treated with conditional media from senescent AML12 cells (24 h) along with or without saturated fatty acids palmitate (0.5 mM for 24 h). Statistical differences were calculated significant as *p<0.05, **p<0.01, and ****p<0.0001.